The Resting State of $P450_{cam}$: A QM/MM Study

Jan C. Schöneboom and Walter Thiel*

Max-Planck-Institut für Kohlenforschung, Kaiser-Wilhelm-Platz 1, D-45470 Mülheim an der Ruhr, Germany

Received: January 29, 2004; In Final Form: March 25, 2004

The substrate-free form of $P450_{cam}$ (CYP101) has been studied by combined quantum mechanical/molecular mechanical (QM/MM) calculations. The central iron(III) aqua porphyrin complex is treated with density functional theory, while the protein/solvent environment is represented by the CHARMM force field. Calculations with different functionals probe the influence of the amount of exact exchange on the relative energies computed for different spin states. B3LYP/CHARMM computations indicate a doublet ground state consistent with experimental results, with small energetic separations to the quartet and sextet. Optimized doublet geometries are in good agreement with experimental data. Comparisons with analogous calculations on the isolated QM system in the gas phase show that the protein/solvent environment reduces the doublet−quartet and doublet−sextet gaps, favors an upright conformation of the axial water ligand by H-bond interactions within the binding pocket, and lengthens the Fe−S bond while shortening the Fe−O bond. Different protein/solvent conformations (obtained from a total of 12 molecular dynamics snapshots in two protonation states) cause notable, but still relatively minor, fluctuations in the computed energetic and structural properties.

1. Introduction

Cytochrome P450 enzymes are a family of ubiquitous metabolizing heme proteins that perform a variety of functions, including biosynthesis of, for example, steroid hormones, as well as detoxification of xenobiotics.[1] In the substrate-free form of P450 enzymes, the heme iron atom is in the ferric (Fe^{III}) state. There has been a longstanding controversy regarding the sixth ligand at the iron atom.[2] X-ray diffraction studies have resolved this issue by proving the presence of an oxygen donor, without being able to distinguish between water and hydroxide. The first corresponding structure was obtained for the bacterial enzyme cytochrome $P450_{cam}$ (CYP101).[3] Subsequent electron−nuclear double resonance (ENDOR) and electron spin−echo envelope modulation (ESEEM) measurements in ^{17}O-enriched water have finally identified water as the sixth ligand.[4,5] The active site environment of $P450_{cam}$ with a cluster of six water molecules filling the binding pocket is depicted in Figure 1.

The ferric ion in $P450_{cam}$ equilibrates between the low-spin (LS) doublet ($S = 1/2$) and the high-spin (HS) sextet ($S = 5/2$) state. Chart 1 displays the corresponding d-orbital occupations and the alternative quartet (intermediate spin, IS) configuration.

It is known experimentally[2,6,7] that the LS state is the ground state of the hexacoordinated resting form (in the absence of a substrate). When the substrate camphor is bound, the water molecules (including the axial water ligand) are expelled from the pocket, resulting in a pentacoordinated iron, with a high-spin ground state. The corresponding shift in redox potential has mechanistic significance: The redox potential of the physiological reductant of $P450_{cam}$, putidaredoxin, allows for a reduction of the substrate-bound ferric high-spin $P450_{cam}$, but not of the ferric low-spin resting form.[8] The (Fe^{III}) LS ground state of the ferric aqua heme complex in P450 enzymes is unexpected, because it is in contrast to the situation in other heme enzymes, such as horseradish peroxidase, cytochrome *c*

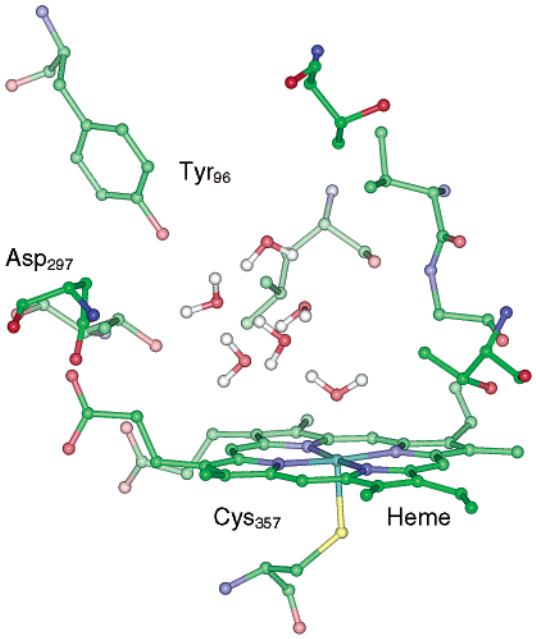

Figure 1. Active site of $P450_{cam}$ in the resting form.

CHART 1

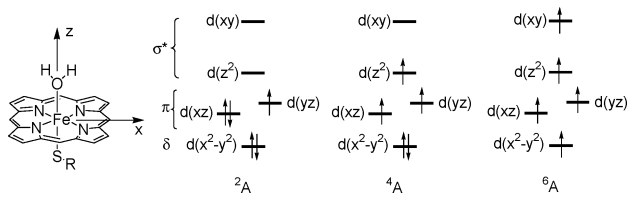

peroxidase, and metmyoglobin.[9] Several known model compounds with water ligands also have a HS ground state.[10]

The origin of the preferred LS configuration in P450 has been investigated by means of quantum mechanical calculations.[9] An early study[11] on [Fe^{III}(protoporphyrinIX)(SMe)(H_2O)] employ-

* To whom correspondence should be addressed. Phone: +49-208-306-2150. Fax: +49-208-306-2996. E-mail: thiel@mpi-muelheim.mpg.de.

10.1021/jp049596t CCC: $27.50
Published on Web 05/11/2004

ing the semiempirical restricted open-shell INDO/S method determined a sextet ground state, however, with a small energy separation of 4 kcal/mol to the doublet and 6 kcal/mol to the quartet state. When the electrostatic interactions of the complex with the enzyme environment were taken into account by adding the surrounding atoms as point charges to the one-electron Hamiltonian, the doublet state became the ground state, in agreement with experimental results. More recently, the origin of the low-spin state found for the resting form has been reexamined by density functional theory (DFT) calculations.[9,12−14] These studies have shown that the relative state energies depend on the functionals and basis sets used; however, they generally favor the low-spin doublet state as the ground state without invoking the electric field of the enzyme environment. Scherlis et al.[15] performed DFT single point calculations using geometries derived from X-ray data and fixed protein point charges in the QM treatment. In accord with previous DFT studies, the doublet state was found to be the ground state. However, in contrast to the results of the earlier INDO/S study,[11] the inclusion of the polarizing effect of the enzyme environment was found to stabilize the quartet state, thus reducing the doublet−quartet gap. Another open question concerns the conformation of the water ligand. While the ESEEM experiment suggests an upright conformation, the model computations favor a "tilted" conformation, where the water protons form hydrogen bonds with the porphyrin nitrogen atoms. This disagreement is probably due to the neglect of suitable hydrogen-bond acceptors in the model computations, which are present in the protein pocket.

A more fundamental problem is the fact that the relative stability of the different spin states depends markedly on the treatment of the exchange interactions.[9,11−14] ROHF calculations (with exact exchange) thus show a clear preference for the sextet as the ground state. On the other hand, the "pure" density functional BLYP (no exact exchange) strongly favors a doublet ground state. Hybrid functionals using the B3 exchange expression due to Becke (20% exact exchange) give smaller energy separations with a slight preference for the doublet state. Such effects have recently been investigated thoroughly[16,17] for Fe^{II} transition metal complexes whose HS−LS splitting depends strongly on the amount of exact exchange included. For complexes with a sulfur-rich first coordination sphere, different density functionals yield results that vary by up to 1 eV. These variations were traced back to the systematic overestimation of the stability of HS states by HF theory, where Fermi correlation is explicitly included through the exchange terms, while Coulomb correlation is not. With density functionals, the HS−LS splitting in transition metal complexes was shown to linearly depend on the coefficient of exact (HF) exchange admixture. While the pure density functionals BP86 or BLYP are strongly biased toward LS states, the popular hybrid functional B3LYP was found to overestimate the stability of HS states. On the basis of these observations and by reference to experimental data, it was suggested to reduce the 20% admixture of HF exchange in the B3 functional to 15%. A corresponding implementation of a density functional with 15% HF exchange, dubbed B3LYP*, correctly predicts the ground-state multiplicity of a range of iron−sulfur complexes, while retaining the overall good accuracy in applications to "standard" systems.[17]

Taken together, the results from previous theoretical studies indicate that geometries as well as relative energies of spin states are sensitive toward the QM treatment and environmental factors. Currently, the method of choice to model effects of the protein is the combined quantum mechanical/molecular mechanical (QM/MM) approach. Herein we present full QM/MM optimizations of a complete model of $P450_{cam}$ to study the influence of the protein environment on the central iron complex, considering the specific interactions of the axial ligand with other water molecules or protein residues in the active site. In this context, we investigate the influence of the amount of the exact exchange admixture in the density functional on the computed doublet−quartet and doublet−sextet gaps of the iron−aqua complex in a comprehensive manner. This will allow us to assess the intrinsic accuracy of the DFT method, which is also of interest with regard to previous model studies.[9,12−14] The paper is organized as follows: In section 2, we present the details of our computational model. The results are given in section 3 and discussed in section 4. Section 5 contains concluding remarks.

2. Computational Details

A. Setup of the System and Strategy. Because the X-ray data available for the substrate-bound complex of $P450_{cam}$ exhibit a significantly better resolution (1.6 Å, PDB code 1DZ4),[18] as compared to the structure of the substrate-free enzyme (2.2 Å, PDB code 1PHC),[3] we have chosen to build the model for our simulations based on 1DZ4. No significant differences in the conformation of the protein backbone or the side chain atoms exist between the two structures, apart from a slight repositioning of the Phe87 side chain.[18] To model the resting state, the camphor molecule was removed and replaced by a cluster of six water molecules from the substrate-free structure.[3] In the latter, only the iron-linked aqua ligand was resolved as an isolated sphere of electron density. The remaining five solvent molecules in the substrate pocket occupy a large lobe of unresolved electron density. Hence, the cluster of water molecules resulting from the refinement procedure represents only one of many energetically similar configurations that coexist. This is probably due to the absence of hydrophilic protein groups in the active site capable of introducing a strong preference for one particular configuration. Therefore, we performed MM molecular dynamics (MD) simulations with CHARMM[19,20] to determine a set of representative configurations of the water cluster and the protein environment. Details of the setup procedure and the MM calculations are presented in the Supporting Information. To assess the influence of different protein conformations on the computed properties, separate QM/MM geometry optimizations were performed for six randomly picked structures denoted snapshots 0−5 (see below) in the doublet, quartet, and sextet states, respectively. To assess the influence of the protein environment on the QM subsystem, full geometry optimizations of the isolated species in the gas phase were performed.

B. Protonation State and Solvation. The assignment of protons to titratable groups of the protein is done according to a previously defined standard protocol,[21] using a built-in procedure of CHARMM (hbuild), published protonation states (based on Poisson−Boltzmann calculations) for $P450_{cam}$,[22] and visual inspection of the environment of charged amino acids and histidine residues. The nonstandard assignments are as follows: (i) Glu366 (an acidic amino acid residue) was protonated at the carboxylate side chain. (ii) The basic amino acids His80, His270, His308, His353, His355 were protonated at both nitrogen atoms. All other histidines are protonated at either the δ- or ϵ-nitrogens upon visual inspection of their environment. (iii) Asp297, an acidic residue situated at the active site next to one of the heme (A) propionate side chains, has been treated as negatively charged in a previous study on compound I of $P450_{cam}$.[21] However, the short distances between

the two carboxylate functions of Asp297 and the A-propionate side chain seen in X-ray structure of the resting state (1PHC)[3] as well as in that of the substrate-bound protein (1DZ4)[18] suggest that these groups are linked by a hydrogen bond, where protonated Asp297 would be the H-bond donor. The distances between the two carboxylate oxygens of Asp297 (OD1, OD2) to the closest oxygen on the propionate (O2A) in 1PHC/1DZ4 are 2.44/2.41 Å (OD1−O2A) and 3.10/3.20 Å (OD2−O2A), respectively. In the present study we have treated Asp297 both as protonated at OD2 (since this atom has the shorter distance to O2A) and as unprotonated, by performing two independent series of MM-MD and subsequent QM/MM geometry optimization calculations (see below). The impact on the resulting QM/MM calculated properties (relative energies, geometries) will be discussed. In the following, the protein containing protonated Asp297 is denoted as protonation state 1 (Prot1), while that with the negatively charged Asp297 is denoted as protonation state 2 (Prot2). Both systems were solvated with a layer of TIP3P water molecules of 16 Å thickness, leading to a system of ca. 28 500 atoms in total, with ca. 21 000 atoms in the solvent. The net charge is −9e (Prot1) or −10e (Prot2).

C. Snapshots. Force field MD (NVT) simulations for Prot1 and Prot2 served to relax the system after solvation and to generate representative protein/solvent conformations. Five randomly picked snapshot structures from each of the two MD trajectories (snapshots 1−5) and the initial structures before MD (snapshot 0) were energy minimized and selected as input structures for the QM/MM study (see Supporting Information). The different protonation states of Asp297 in Prot1 and Prot2 give rise to significant differences in the geometry of the H-bond network around this amino acid and the heme A-propionate side chain (amino acids Asp297, Arg299, Tyr75, and Gln322) during the force field calculations. In the case of Prot1, this network is maintained and corresponds qualitatively to the X-ray structure: Apart from a slight repositioning of the Asp297 side chain during the initial energy minimization, all structures exhibit qualitatively the same geometric features. There is one H-bond between Asp297 and the heme A-propionate (from OD2 to O2A), the distances varying from 2.64 to 2.69 Å (OD2−O2A) and 3.49 to 3.64 Å (OD1−O2A) in the six snapshots. Turning to Prot2, where there is no hydrogen bond, the negatively charged Asp297 side chain rotates to avoid interaction with the heme A-propionate (this occurs already during the initial optimization); here the distances range from 3.74 to 4.26 Å (OD2−O2A) and 3.44 to 3.70 Å (OD1−O2A). In the snapshot structures 1−5, which result from MD, a water molecule (WAT63) has changed its position to a bridging conformation between the negative carboxylates of Asp297 and the A-propionate, thereby forming two hydrogen bonds that stabilize the relative position of the two negative groups. However, the repositioning of Asp297 in Prot2 disturbs the geometry of neighboring amino acids, as is obvious from the root-mean-square deviation (rmsd) calculated for Asp297, Arg299, Tyr75, and Gln322 in snapshots 0−5 (see Figure 2). This shows that there is an increasing difference in the geometry of these amino acids with respect to snapshot 0, the rmsd increasing to 0.83 Å in snapshot 5. In contrast, the structures with the protonated Asp297 (Prot2) have a maximum rmsd of 0.35 Å at snapshot 3. The smaller rmsd reflects the finding that the relative orientation of these groups is essentially preserved due to the presence of a stable H-bond network.

The fact that Prot1 shows an H-bond pattern that is stable during MD and is close to the X-ray structure makes this protonation state the more realistic choice. We nevertheless report QM/MM results for both protonation states, because (i) the impact of different protonation states in the MM environment on the QM region is of interest and (ii) Prot2 has been employed in a previous QM/MM study on $P450_{cam}$.[21] We note that the distance from the Asp297 carboxylate group to the nearest QM atom is ca. 6 Å and that there are no direct steric interactions between Asp297 and the QM region. The perturbation arising from the two different protonation states on the QM part may thus be expected to be small.

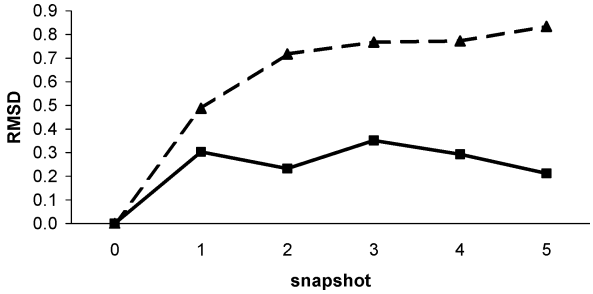

Figure 2. Root-mean-square deviation (Å) within the H-bond network around Asp297 (Asp297, Arg299, Tyr75, Gln322) of snapshots 1−5 for Prot1 (solid line, squares) and Prot2 (broken line, triangles). Reference is the X-ray structure after addition of hydrogen atoms and solvent water and subsequent energy minimization.

D. QM/MM Calculations. The general QM/MM methodology adopted in the present study is documented extensively in refs 21 and 23. In the following, we only describe the aspects relevant to the present work.

QM Methods. The QM part was treated with unrestricted Kohn−Sham DFT. We have employed different density functionals for the exchange energy to assess the influence of the amount of HF exchange on the relative energies of the spin states (doublet, quartet, sextet) of the central iron(III)−aqua complex (see Scheme 1). Geometry optimizations were performed with the B88[24] (no HF exchange) and B3[25] (20% HF exchange) functionals. Additional single-point calculations were done with the Becke half-and-half functional[26] (50% HF exchange). The correlation energy was calculated from the LYP functional[27] in all cases. The doublet state was represented by an unrestricted Slater determinant corresponding to the electronic configuration shown in Scheme 1 (^{2}A state). Because of the small energetic separation between the frontier orbitals and the high local symmetry of the system, it is conceivable that the chosen occupancy corresponds to an excited doublet state; however, time-dependent DFT calculations with the B3LYP functional yielded only positive excitation energies and thus confirmed that the chosen configuration is indeed the doublet ground state. The computed S^2 expectation values for the doublet were typically 0.8−0.9 (ideally 0.75), indicating only minor spin contamination, while the quartet and sextet states were found to be essentially pure spin states. We have therefore not corrected the calculated multiplet energies by any of the available spin projection schemes.

QM Regions and Basis Sets. In the QM/MM calculations, two different QM regions R1 and R2 were employed, shown in Figure 3. These QM subsystems comprise the following set of atoms: (i) R1 (42 QM atoms): iron−oxo−porphyrin (without side chains of the heme), the sulfur of Cys357, and the axial water ligand. In the gas-phase calculations, this corresponds to [FeO(SH)(porph)(H_2O)]. (ii) R2 (59 QM atoms): iron−oxo−porphyrin (without side chains of the heme), Cys357, the CO group of Leu346, the NH−C^{α}H unit of Leu348, and the axial water ligand. The basis sets used in the present investigations are abbreviated as B1 and B2. The iron atom is always described

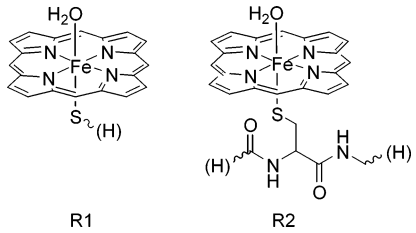

Figure 3. QM regions R1 and R2.

by a small-core effective core potential and the associated LACVP basis of a double ζ quality.[28] Basis B1 employs a 6-31G basis on all other atoms. Basis B2 additionally contains a set of polarization and diffuse functions (6-31+G*) on the six atoms coordinated to iron and a set of polarization and diffuse functions on the two protons of the axial water ligand (6-31++G**).[29] In the following, the QM level employed in a particular QM/MM calculation will be denoted by the expression QM region/basis set, e.g. R1/B1 or R2/B2. Extensive QM/MM studies on different snapshots were carried out with the smaller QM region R1 and basis B1. QM/MM calculations using the larger QM region R2 and basis B2 were done for snapshot 5 (Prot1) and snapshot 4 (Prot2), which exhibit the lowest energy.

QM/MM Methods. An electronic embedding scheme[30] was applied, i.e. the fixed MM charges were included into the one-electron Hamiltonian of the QM calculation and the QM/MM electrostatic interactions were evaluated from the QM electrostatic potential and the MM atomic charges. No cutoffs were introduced for the nonbonding MM and QM/MM interactions. To treat the QM/MM boundary, we used hydrogen link atoms with the charge shift model.[31,32]

Geometry Optimization. The QM/MM optimizations included the heme, the six water molecules in the binding pocket, and the following set of residues of the active site: Tyr75, Phe87, Tyr96, Pro100, Thr101, Gln108, Arg112, Val119, Leu244, Leu245, Gly249, Thr252, Val253, Leu294, Val295, Asp297, Arg299, Gln322, Thr349, Phe350, Gly351, His355, Leu356, Cys357, Leu358, Gly359, Gln360, Leu362, Ala363, Ile367, Wat63, and Wat257. This corresponds to a total of 586 optimized atoms. Due to the high conformational complexity of the system, separate geometry optimizations for individual spin states often lead to differences in conformations that are not related to the characteristics of the central iron complex but to the protein/solvent environment. To avoid corresponding artifacts, we first performed QM/MM geometry optimizations for the doublet state. These geometries then served as the starting point for geometry optimizations of the quartet and sextet states.

Codes. For the QM treatment in the QM/MM as well as in the pure QM calculations we employed the TURBOMOLE program.[33] All QM/MM calculations were performed with the ChemShell package.[23,34] The CHARMM22 force field[20] run through the DL-POLY program[35] was used for the treatment of the MM part of the system. Geometry optimizations were performed with the HDLC optimizer,[36] which is part of ChemShell.

3. Results

A. The Influence of Exact Exchange. To demonstrate the influence of the amount of HF exchange on the calculated relative energies of different spin states, we have calculated relative energies obtained with the B88,[24] B3,[25] and BH[26] exchange expressions in the ^{2}A, ^{4}A, and ^{6}A states, using the large QM region R2 and basis set B2. The LYP functional[27] was used for the computation of the correlation energy in all cases. The corresponding equilibrium geometries of the different spin states obtained with B3LYP are shown in Figure 4, for both the QM system in the protein environment as well as isolated in the gas phase. QM/MM optimizations refer to snapshot 4 (Prot2). The doublet species has an Fe−O bond with a bond length of 2.141 (2.241) Å in the protein (gas phase). For the quartet and sextet states, the Fe−O interaction is repulsive, leading to significantly larger bond distances: QM/MM optimizations predict distances of 2.475 (quartet) and 2.467 (sextet) Å in the enzyme. In the gas phase, the Fe−O bond is broken and the water ligand detached from iron in both the IS and HS states. In these structures, the water molecule is loosely attached to the heme via a hydrogen bond to one of the pyrrole nitrogens.

The relative energies shown in Figure 5 include adiabatic energies of the doublet (D), quartet (Q), and sextet (S) species at equilibrium geometries (relative to the doublet), as well as vertical energies of the other two electronic states at a given equilibrium geometry. We have chosen to report BLYP and BHLYP single-point energies on B3LYP-optimized geometries in all cases, because, at this stage, we are primarily interested in the effect of HF exchange on electronic energies, i.e., the intrinsic preference of a given functional for the HS, IS, or LS situation. Relative energies from separately optimized structures would include geometry relaxation effects, which may yield misleading results if the geometries obtained from different functionals are qualitatively different, i.e., not consistent. For example, the quartet−doublet gap from separate R1/B1 geometry optimizations in the gas phase using the B3LYP and BLYP functionals, respectively, is 5 and 4 kcal/mol. However, the optimized geometries of the ^{4}A state are very different: while the B3LYP-optimized structure features a weak Fe−O interaction, BLYP predicts the axial water to be completely unbound. The close agreement of the calculated quartet−doublet gaps is thus coincidental, since the two functionals predict qualitatively different equilibrium structures for the ^{4}A state in the gas phase.

An overall inspection of Figure 5 shows that the energy ordering for a given functional is qualitatively similar in the protein (a) and the gas phase (b), with minor quantitative variations. The following assessment of the different functionals will therefore focus on the situation in the protein; the differences between protein and gas-phase results will be discussed in more detail in section 3B.

In the protein (Figure 5a), the QM/MM calculations with the B3LYP functional (20% HF exchange) predict the global minimum to be the doublet species, which is more stable than the other optimized spin states by 2.4 kcal/mol (quartet) and 3.3 kcal/mol (sextet). Essentially the same relative energies are obtained from R2/B2 single point energy calculations on geometries optimized with the smaller QM region R1 and basis set B1: the quartet (sextet) species is computed at 1.9 (3.4) kcal/mol above the doublet. Analogous single point calculations on the alternative protonation state of Asp297 (Prot1, see above) lead to the same energy ordering, with relative QM/MM energies of 0.8 (quartet) and 2.8 (sextet) kcal/mol (see section 3B for further discussion of the protonation states). Considering the vertical stabilities of the three spin states at optimized B3LYP/CHARMM geometries (see Figure 5a), the relatively small structural changes between the three spin states are sufficient to change the energy order from D < Q < S (doublet geometry) to Q < D < S (quartet geometry) and S < Q < D (sextet geometry). In ligand field theory nomenclature, this indicates a change from a "strong ligand field" to a "weak ligand field". The corresponding geometrical change that is most relevant in

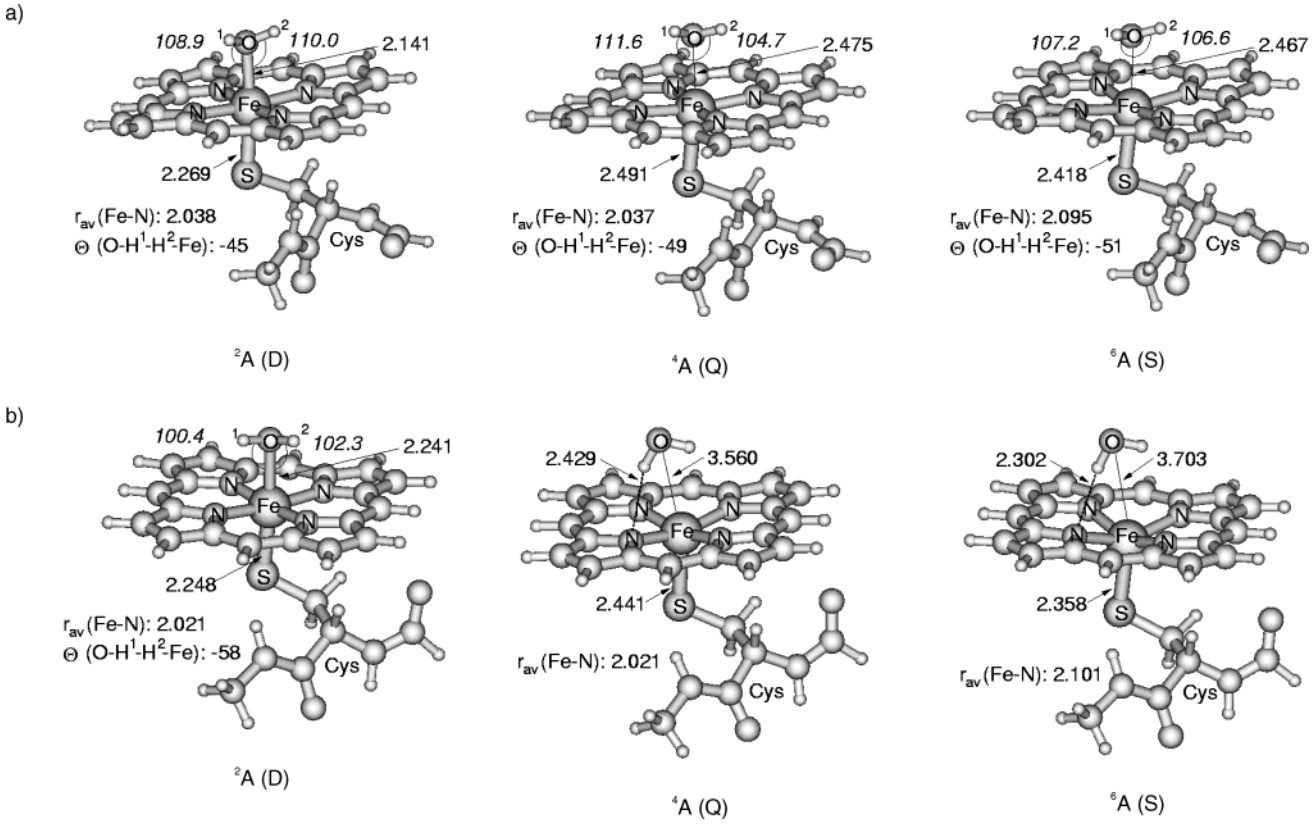

Figure 4. Optimized geometries, QM region R2, basis B2. Bond lengths in Å, angles (oblique numbers) in degrees. Improper dihedral angle Θ in degrees. (a) Protein: snapshot 4 (Prot2), B3LYP/CHARMM. (b) Gas phase: B3LYP.

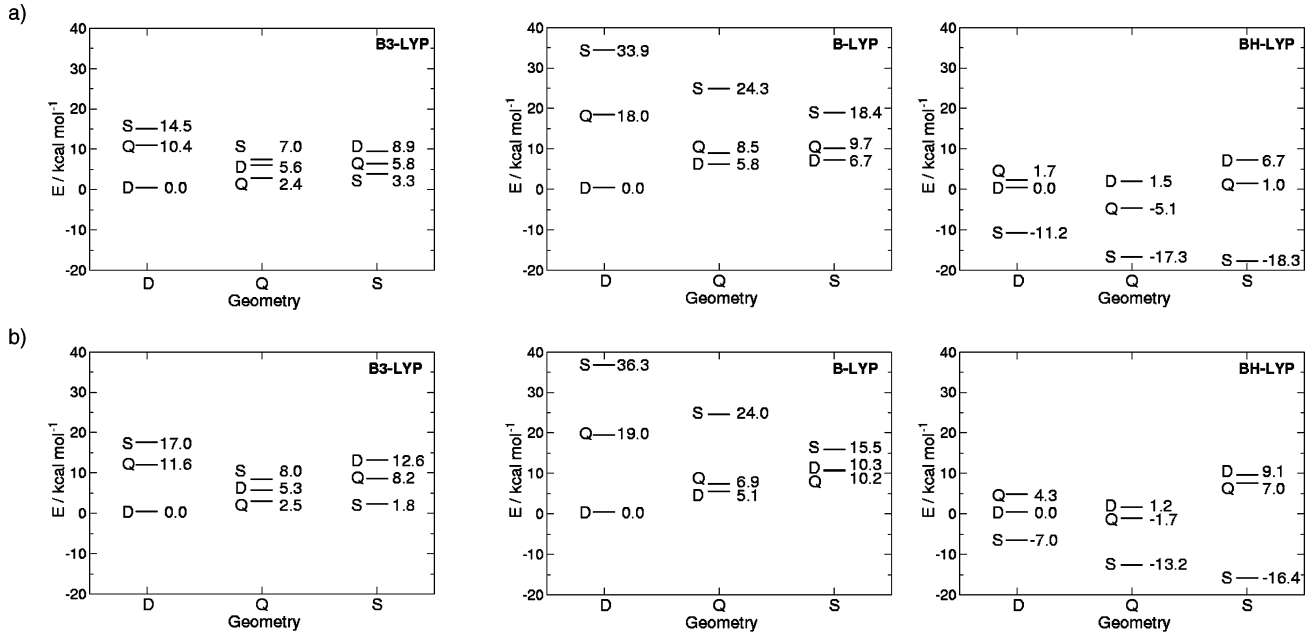

Figure 5. Adiabatic and vertical relative energies (kcal/mol) of the doublet (D), quartet (Q), and sextet (S) state, computed with three different exchange density functionals (B, B3, BH), QM region R2, basis B2. (a) Protein: relative QM/MM energies, B3LYP/CHARMM-optimized geometries, snapshot 4 (Prot2). (b) Gas phase: relative QM energies, B3LYP-optimized geometries.

this connection is the lengthening of the Fe−O bond, i.e., the detachment of water from the heme iron (see Figure 4). The calculated B3LYP energies are consistent with the experimental finding that the ground-state multiplicity changes from doublet to sextet upon binding of substrate and the associated expulsion of water molecules from the active site.

The BLYP energies (no HF exchange) exhibit a clear preference for the doublet state, giving the ordering of the spin states as D < Q < S at all three considered geometries. Comparing the resulting adiabatic relative energies with the B3LYP data, the quartet and sextet states are destabilized by 6 and 15 kcal/mol, respectively. In contrast, increasing the fraction of exact exchange from 20% (B3) to 50% (BH) lowers these states by 8 and 22 kcal/mol. Here, the sextet state is calculated below quartet and doublet at all geometries. The stabilization of the IS and HS states with increasing fraction of HF exchange is approximately equally pronounced in the protein and the gas phase. Hence, similar to published results for Fe^{II}−sulfur

TABLE 1: Relative Energies (kcal/mol) of the ^{4}A State with Respect to the ^{2}A State (QM Region R1, Basis B1)

	B3LYP				BLYP	
	Prot1		Prot2		Prot2	
snapshot	$\Delta E^{QM/MM}$	ΔE^{QM}	$\Delta E^{QM/MM}$	ΔE^{QM}	$\Delta E^{QM/MM}$	ΔE^{QM}
0	−1.83	−5.62	0.73	−2.32	7.04	4.12
1	0.85	−2.71	1.06	−1.99	7.58	4.46
2	−0.07	−2.81	−0.29	−2.38	5.98	3.85
3	−0.31	−2.71	0.73	−1.01	6.86	5.03
4	0.12	−2.09	0.57	−2.41	6.91	4.58
5	−1.12	−2.82	−0.62	−1.62	0.39[a]	4.05[a]
average[b]	−0.39 ± 0.77	−3.13 ± 1.02	0.36 ± 0.54	−1.95 ± 0.45	6.87 ± 0.51	4.41 ± 0.40
gas phase		5.48		5.48		4.16[c]

[a] Not comparable due to different conformations in the MM environment: two of six water molecules in the binding pocket reorient in this BLYP/MM optimization, which gives rise to a different and more stable H−bond network and thereby to an artificially low QM/MM energy gap. [b] With confidence interval 2σ. [c] Not directly comparable to the B3LYP value, since the axial water ligand dissociates during the BLYP gas−phase optimization of the quartet state; BLYP single−point calculations at B3LYP-optimized geometries yield a doublet−quartet gap of 10.9 kcal/mol (see section 3A for analogous results at the R2/B2 level).

TABLE 2: Relative Energies (kcal/mol) of the ^{6}A State with Respect to the ^{2}A State (QM Region R1, Basis B1)

	B3LYP				BLYP	
	Prot1		Prot2		Prot2	
snapshot	$\Delta E^{QM/MM}$	ΔE^{QM}	$\Delta E^{QM/MM}$	ΔE^{QM}	$\Delta E^{QM/MM}$	ΔE^{QM}
0	1.43	0.11	4.95	4.00	20.01	18.78
1	3.71	2.50	4.32	4.15	19.82	18.89
2	3.51	3.36	3.53	3.81	18.48	18.41
3	2.80	3.08	3.65	4.78	18.86	19.29
4	2.78	2.98	4.01	4.50	18.95	19.24
5	2.87	3.17	3.78	4.15	18.05	19.30
average[a]	2.85 ± 0.65	2.53 ± 1.00	4.04 ± 0.56	4.23 ± 0.47	19.03 ± 0.62	18.98 ± 0.29
gas phase		6.92		6.92		20.51

[a] With confidence interval 2σ.

complexes[16] and model compounds of the resting form of P450,[9] we find large variations of the relative stabilities of the IS and HS vs the LS states, depending on the amount of HF exchange in the density functional. As noted above, it is known[16,17,37] that pure density functionals such as BLYP are strongly biased toward LS states, whereas B3LYP tends to overestimate the stability of HS states, and it has therefore been recommended[16] to reduce the amount of exact exchange in the B3LYP functional from 20% to 15%. Instead of choosing this pragmatic approach, we apply the standard B3LYP functional in the following, which is rather close to the recommended ideal admixture of HF exchange. In addition, we report results obtained with the BLYP functional, which may serve as an "upper bound" for estimating the stability of the LS states.

B. Influence of the Protein Environment. *Relative Energies.* Tables 1 and 2 summarize the energies of the optimized ^{4}A and ^{6}A species relative to the corresponding ^{2}A minima, respectively, computed using the B3LYP and BLYP functionals for the smaller QM region R1 and basis set B1. The relative QM/MM energies ($\Delta E^{QM/MM}$) are the sum of the contributions from the QM (ΔE^{QM}) and the MM (ΔE^{MM}) treatment. ΔE^{QM} contains the electrostatic interactions between the QM region and the MM point charges, and ΔE^{MM} includes the van der Waals interactions between QM and MM atoms (evaluated at the force field level).

The entries in Tables 1 and 2 show the influence of different protein conformations (snapshots 0−5) and the two different protonation states (Prot1, Prot2) on the calculated state energy differences. Generally, the fluctuations in $\Delta E^{QM/MM}$ are rather small, at most 3 kcal/mol. The QM/MM doublet−quartet gaps obtained with the B3LYP functional vary from −2 to 1 kcal/mol in different snapshots, while the corresponding BLYP results range from 6 to 8 kcal/mol. The sextet state is always calculated at higher energy; QM/MM relative energies lie between 2 and 5 kcal/mol for B3LYP (18−20 kcal/mol at the BLYP level). The QM contributions ΔE^{QM} to the doublet−quartet gap are generally lower than the $\Delta E^{QM/MM}$ values by typically 2−3 kcal/mol, indicating that the MM contributions ΔE^{MM} favor the doublet by this amount. In the case of the doublet−sextet splitting, $\Delta E^{QM/MM}$ and ΔE^{QM} are generally closer to each other.

Figure 6 shows a graphical summary of the B3LYP-based relative energies in the different snapshots. Inspection of this figure and of the data in Tables 1 and 2 indicates that these relative energies are not affected much by the choice of protonation state (Prot1, Prot2). The doublet−quartet and doublet−sextet gaps are apparently lower by about 1 kcal/mol in Prot1 (protonated Asp297), but the fluctuations in the results are of a similar order, and clearly more snapshots would need to be examined for a proper statistical analysis.

In accord with previous DFT gas-phase model studies,[9,12−14] we obtain a doublet ground state for the isolated species with both functionals employed. At the R1/B1 level, the B3LYP gas-phase calculations predict that the quartet and sextet minima are 5.5 and 6.9 kcal/mol higher in energy, respectively. As noted before,[11,15] the protein has a significant influence on the relative stability of the spin states. According to the B3LYP/MM (R1/B1) results, the quartet is stabilized relative to the doublet by about 5−6 kcal/mol (see average values for Prot2 and Prot1 in Table 1). This is mainly caused by the QM contributions (ΔE^{QM}), which favor the quartet by about 7−9 kcal/mol (see section 4 for a detailed analysis), whereas the MM contributions (ΔE^{MM}) exert a counteracting effect of 2−3 kcal/mol that is due to many subtle variations in the MM environment and thus cannot be attributed to dominant individual interactions. The sextet is also stabilized relative to the doublet, but to a lesser

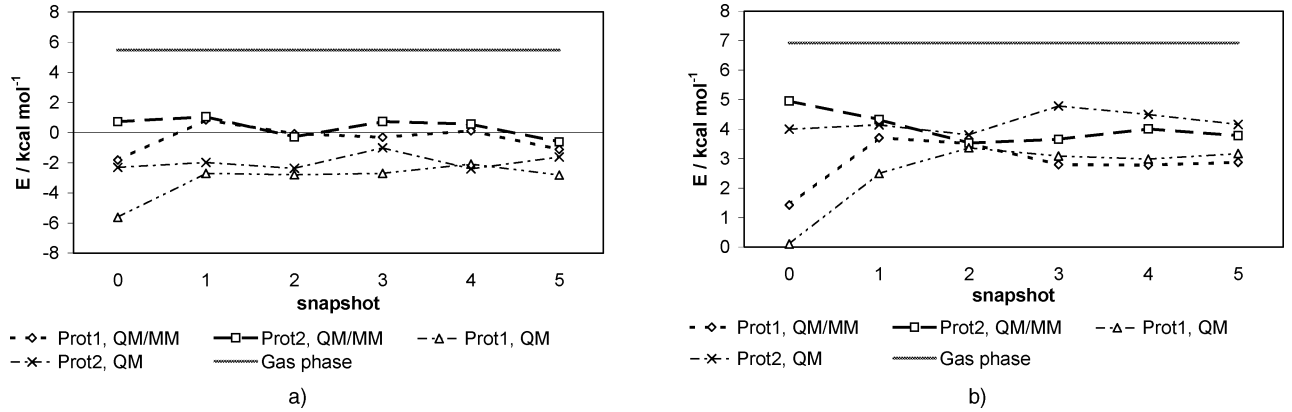

Figure 6. Relative QM/MM energies and QM contributions (kcal/mol) with respect to the ^{2}A state (B3LYP, QM region R1, basis B1): (a) ^{4}A state and (b) ^{6}A state.

TABLE 3: Selected Geometrical Parameters from R1/B1 Geometry Optimizations in the Enzyme Environment (Snapshots 0−5) and in the Gas Phase (QM Region R1, Basis B1)[a,b]

		r^{av}(Fe−N)		r(Fe−O)		r(Fe−S)		θ^{av}(Fe−O−H)		Θ(O−H−H−Fe)[c]	
	snapshot										
^{2}A	0	2.030	2.028	2.061	2.011	2.351	2.348	108.9	115.2	45.3	31.6
	1	2.031	2.030	2.084	2.025	2.328	2.349	110.8	114.0	40.0	33.9
	2	2.029	2.032	2.085	2.023	2.347	2.365	109.8	119.0	42.2	22.2
	3	2.030	2.031	2.092	2.043	2.357	2.353	111.1	114.4	40.4	33.5
	4	2.033	2.031	2.100	2.032	2.353	2.356	110.1	115.8	42.4	30.5
	5	2.031	2.030	2.103	2.035	2.361	2.358	113.5	115.4	35.9	31.3
	mean	2.031	2.030	2.088	2.028	2.350	2.355	110.7	115.6	41.0	30.5
	gas phase	2.019		2.114		2.290		108.1		46.0	
^{4}A	0	2.030	2.028	2.334	2.268	2.551	2.545	104.7	109.5	53.3	44.7
	1	2.032	2.031	2.365	2.277	2.503	2.543	106.0	110.4	50.0	42.8
	2	2.029	2.032	2.387	2.297	2.526	2.554	105.8	112.0	50.6	40.0
	3	2.030	2.031	2.379	2.280	2.542	2.567	108.6	114.2	45.8	36.0
	4	2.033	2.031	2.393	2.280	2.534	2.567	105.5	114.2	51.4	36.0
	5	2.030	2.030	2.389	2.293	2.557	2.572	113.3	115.9	37.2	32.9
	mean	2.031	2.031	2.375	2.283	2.536	2.558	107.3	112.7	48.1	38.7
	gas phase	2.201		2.554		2.479		94.3		70.6	
^{6}A	S0	2.082	2.080	2.268	2.235	2.494	2.493	107.9	110.7	48.0	42.3
	S1	2.086	2.084	2.345	2.278	2.448	2.484	107.4	107.0	47.5	48.5
	S2	2.083	2.083	2.348	2.242	2.474	2.519	106.8	118.9	48.7	25.4
	S3	2.085	2.086	2.354	2.276	2.482	2.496	108.6	112.0	45.8	39.7
	S4	2.088	2.085	2.361	2.251	2.478	2.503	106.5	115.4	49.6	33.2
	S5	2.082	2.083	2.345	2.262	2.501	2.510	112.8	114.1	38.0	35.9
	mean	2.084	2.084	2.337	2.257	2.480	2.501	108.3	113.0	46.3	37.5
	gas phase	2.086		2.493		2.417		94.7		69.6	

[a] Distances r in Å, and angle θ and improper torsional angle Θ in deg). [b] The two QM/MM values come from separate optimizations of protonation state 1 and 2 (first and second column, respectively). [c] Absolute values. The oxygen and hydrogen atoms belong to the axial water ligand.

extent, by about 3−4 kcal/mol (see average B3LYP-based values for Prot2 and Prot1 in Table 2). In this case, essentially the whole stabilization comes from the QM contributions.

As a consequence of the interactions with the environment, the three spin states move closer to each other in energy compared to the gas phase. The average values from the B3LYP/MM (R1/B1) calculations for Prot1 and Prot2 suggest that the doublet and quartet states are essentially degenerate in the enzyme (within the statistical fluctuations; see Table 1). The use of the larger QM region R2 and the larger basis set B2 for the lowest energy snapshot 4 (Prot2) favors the doublet by about 2 kcal/mol over the quartet (compared with R1/B1). An analogous reasoning places the doublet about 3 kcal/mol below the sextet, so our best B3LYP-based estimate for the energy ordering in the resting state of $P450_{cam}$ is D < Q < S (0 < 2 < 3 kcal/mol). As discussed previously (see section 3A), BLYP overestimates the stability of low-spin species, and it is thus not surprising that BLYP predicts the same sequence D < Q < S with larger energy differences (0 < 7 < 19 kcal/mol for R1/B1, and even somewhat higher values after including R2/B2-based corrections). These BLYP relative energies should be considered as upper bounds, and the experimental values are expected to be closer to the B3LYP than the BLYP results.

In summary, our QM/MM results show that the protein environment stabilizes the sextet and particularly the quartet relative to the doublet state such that all three states are rather close in energy. Our best theoretical estimate gives a doublet ground state consistent with the experimental findings, but it should be stressed that the corresponding numerical results should be viewed with some caution because of the limitations in the intrinsic accuracy of the DFT/MM approach and in the sampling of conformational space.

Geometries. Key features of the optimized geometries from the R1/B1 calculations in the enzyme environment (B3LYP/MM) as well as the isolated gas-phase systems (B3LYP) are summarized in Table 3.

The differences in the electronic structures of the various spin states are reflected in their optimized geometries. The doublet state exhibits the shortest bonds of the six ligands to the central iron atom. In contrast, the quartet state has significantly elongated bonds to the axial ligands. This is due to the occupation of the iron d(z^2) orbital, which contributes to the

TABLE 4: Atomic Spin Densities from R1/B1 Geometry Optimizations in the Enzyme Environment (Snapshots 0−5) and in the Gas Phase (QM Region R1, Basis B1)[a]

		r(Fe)		r(O)		r(S)		r^{gr}(por)[b]		r^{av}(N)[c]	
^{2}A	mean[d]	1.16	1.13	−0.002	0.003	−0.08	−0.06	−0.08	−0.08	−0.03	−0.03
	min[e]	1.14	1.11	−0.006	0.002	−0.09	−0.06	−0.09	−0.08	−0.03	−0.03
	max[f]	1.17	1.14	0.001	0.004	−0.06	−0.05	−0.07	−0.07	−0.03	−0.03
	gas phase	1.09		0.001		−0.01		−0.09		−0.02	
^{4}A	mean[d]	2.71	2.74	0.032	0.037	0.30	0.27	−0.03	−0.04	−0.03	−0.04
	min[e]	2.69	2.72	0.028	0.034	0.27	0.25	−0.04	−0.05	−0.04	−0.04
	max[f]	2.73	2.75	0.043	0.045	0.32	0.29	−0.03	−0.04	−0.03	−0.04
	gas phase	2.56		0.021		0.46		−0.03		−0.02	
^{6}A	mean[d]	4.05	4.07	0.037	0.043	0.34	0.32	0.57	0.58	0.12	0.11
	min[e]	4.04	4.06	0.032	0.039	0.32	0.30	0.57	0.57	0.11	0.11
	max[f]	4.07	4.08	0.051	0.050	0.36	0.33	0.59	0.58	0.12	0.12
	gas phase	3.99		0.028		0.49		0.51		0.11	

[a] The two QM/MM values come from separate optimizations of protonation state 1 and 2 (first and second column, respectively). [b] The sum of individual atomic contributions of the porphyrin macrocycle. [c] The average value of the four pyrrole nitrogens. [d] The mean value calculated for snapshots 0−5. [e] The minimum value of snapshots 0−5. [f] The maximum value of snapshots 0−5.

antibonding σ^* orbital along the S−Fe−O axis. In the sextet state, an unpaired electron additionally occupies the iron d(xy) orbital. This orbital mixes with sp^2 orbitals of the pyrrole nitrogens to give a strongly antibonding Fe−N σ^* MO. As a consequence, the Fe−N bonds are lengthened by ca. 0.05 Å and the central iron atom is displaced from the heme plane toward the proximal face of the heme. The improper torsional angle Θ(O−H−H−Fe) is a measure of the tilting of the water ligand with respect to the heme plane. A value of 0° indicates a perfectly upright conformation, with the plane spanned by the three water atoms perpendicular to the heme plane. As obvious from Table 3, the QM/MM optimizations always predict some deviation from the upright geometry, even in snapshot 0, which is optimized starting from the X-ray conformation. This deviation is smallest for the doublet species and slightly more pronounced for the quartet and sextet equilibrium structures.

There are also notable differences in geometry arising from different snapshots. For example, the Fe−O bond lengths vary by up to (D/Q/S) 0.042/0.059/0.093 Å in different snapshots. This is in line with the variances in the calculated relative energies of the three spin states. Comparing the two protonation states (Prot1 vs Prot2), it is obvious that there are some systematic differences related to the conformation of the axial water ligand. For example, the Fe−O bond length is generally longer in Prot1, the average value being (D/Q/S) 0.059/0.092/0.080 Å larger compared to that of Prot2. We attribute these differences to the H-bond interactions between the water molecules in the binding pocket and the axial water ligand: In all Prot1 snapshots, the axial water is engaged in two H-bonds with neighboring (but varying) waters, while in Prot2, there is always only one such H-bond interaction. The stronger attractive interactions with surrounding water on the distal side of the heme in Prot1 apparently elongate the ("competing") Fe−O bond. It is possible that Asp297 (protonated in Prot1 but unprotonated in Prot2) indirectly induces these changes via its H-bond contacts with water in the binding pocket. However, this question should be addressed by MD with extensive sampling of conformations, which is beyond the scope of the present QM/MM study.

More significant are the observed differences between the geometries optimized in the enzyme environment and those for the isolated QM subsystem in the gas phase. This is especially true for the Fe−O bond length, which is generally shorter in all snapshots (Prot1 and Prot2) than in the isolated species. In contrast, the Fe−S bond is elongated in the enzyme environment. For example, the mean Fe−S bond lengths in Prot1 are larger than in the gas-phase species by (D/Q/S) 0.060/0.057/0.063 Å. Moreover, the water ligand is strongly tilted (R1/B1) or even detached from the iron (R2/B2) in the quartet and sextet gas-phase minimum geometries. In these structures, the water protons form hydrogen bonds with the pyrrole nitrogen atoms of the porphyrin. These interactions are not present within the protein environment, where they are replaced with hydrogen bonds to the neighboring water molecule occupying the pocket. Hence, our calculations indicate that the interaction of the axial water ligand with the other water molecules present in the active site favors the upright conformation of this ligand and shortens the Fe−O bond. This effect is apparent in all spin states, but it is most pronounced in the quartet and sextet species.

Our best structural estimates for the system in the enzyme environment from B3LYP/CHARMM22 geometry optimizations (see Figure 4) employing the large QM region R2 yield Fe−O distances of 2.141/2.475/2.467 Å in the doublet/quartet/sextet states, respectively. The computed Fe−S bond lengths at this level of theory are 2.269/2.491/2.418 Å. Hence, the optimized doublet geometry agrees reasonably well with the experimental values[3] of 2.28 Å for the Fe−O and 2.25 Å for the Fe−S bond lengths (estimated uncertainty of the X-ray structure ±0.2 Å). We note that in this geometry, the Fe−H distances to the protons of the axial water ligand are 2.646 and 2.620 Å, in perfect agreement with the estimated distance of 2.62 Å obtained in an ESEEM experiment.[5]

In summary, the QM/MM optimizations employing the large QM region R2 and basis B2 in conjunction with B3LYP/CHARMM22 lead to a geometry for the doublet species in good agreement with the experimental data. A comparison of the geometries from the QM/MM study with corresponding optimizations in the gas phase shows that the enzyme environment shortens the Fe−O bond and favors the upright conformation of the axial water ligand. This is especially pronounced in the quartet and sextet states. In contrast, the Fe−S bond is slightly elongated under the influence of the surrounding protein. Different snapshot structures representing different protein conformations (and protonation states of Asp297) show notable, but relatively small, geometrical variations in the coordination sphere of the iron atom.

Spin Densities. Unpaired spin densities from the B3LYP/CHARMM calculations on the various snapshots and from B3LYP calculations on the isolated gas-phase system are presented in Table 4. Since all snapshots optimized at the QM/MM level show only minor variations in computed spin densities, we give only the average, minimum, and maximum values from the six snapshots. The spin density distribution of the doublet state shows that the unpaired electron is predomi-

nantly localized on the iron atom. This is expected for the single occupation of the d(*yz*) orbital, which has weak interactions with ligand orbitals. In contrast, the quartet state exhibits a significant amount of positive spin density on the sulfur atom, due to the mixing of the iron d(z^2) with the sulfur p(*z*) orbital. In the sextet state, only four equivalents of the five unpaired electrons are attributed to the iron center. This is a result of the strong interaction of the iron d(*xz*) orbital with sp^2 orbitals at the pyrrole nitrogen atoms. These four nitrogen atoms each carry an average spin density of 0.1 e in the sextet state (see last column in Table 4). A comparison of the QM/MM results with the gas-phase calculations of the isolated R1/B1 system reveals a significant redistribution of spin density between the iron and sulfur atom in the quartet and sextet states: Going from the enzyme environment to the gas phase, the sulfur atom aquires more spin density (quartet, 0.30 → 0.46; sextet, 0.34 → 0.49), with a concomitant reduction of spin density on iron (quartet, 2.71 → 2.56; sextet, 4.05 → 3.99). This finding indicates that the protein environment, by polarization and the presence of H-bond donors in the proximal pocket, effects a stabilization of electron density on the sulfur atom. As discussed previously,[21] a similar effect has been observed for the ratio of sulfur vs porphyrin radical character of compound I of P450. Interestingly, the unpaired spin density on the oxygen atom of the axial water ligand is relatively small in all calculations. The mixing of the iron d(z^2) and the oxygen p(*z*) orbitals that yields the singly occupied antibonding σ^*(Fe−O) orbital thus is apparently rather weak.

4. Discussion

The present QM/MM calculations give a doublet ground state for the ferric resting state of P450, in agreement with the experimental assignment.[6−8] The best B3LYP/CHARMM estimates place the quartet state ca. 2 kcal/mol above and the sextet state ca. 3 kcal/mol above the doublet. Since the B3LYP functional is known to underestimate the stability of the LS state due to the admixture of exact exchange (see section 3A), the true energy differences are expected to be even slightly larger. The relatively small energy separations conform with the experimental finding that the ground state (doublet) is in equilibrium with the higher spin states.[6,7] The optimized geometries of the doublet ground state obtained from B3LYP/CHARMM (R2/B2) calculations yield an Fe−O distance of 2.141 Å and an Fe−S bond length of 2.269 Å, which agree well with the X-ray data of 2.28 (±0.2) Å and 2.25 (±0.2) Å, respectively. The computed Fe−H distances to the protons of the axial water ligand are 2.646 and 2.620 Å, in excellent agreement with the value of 2.62 Å obtained from ESEEM measurements.[5] We note that other properties are also calculated in good agreement with experiment, e.g., ^{1}H and ^{14}N hyperfine coupling constants of ligand atoms; this will be the subject of a separate paper.[38] These results support the reliability of the QM/MM approach in predicting the geometrical and electronic features of the iron complex in the enzyme environment.

The protein environment affects the computed properties of the Fe^{III}−aqua complex as follows: (i) The polarization of the QM part by the enzyme environment significantly stabilizes the quartet relative to the doublet state and, to a smaller extent, also the sextet state. (ii) The QM/MM geometries show a preference for conformations with a less tilted axial water ligand, although a perfectly upright conformation with respect to the heme plane is not achieved. The protein/solvent environment favors a significant shortening of the Fe−O bond. In contrast, the isolated species have long Fe−O distances and the axial water ligand nearly parallel to the heme plane (R1/B1) or even completely detached from iron (R2/B2), with the water protons forming hydrogen bonds to the pyrrole nitrogens of the porphyrin. (iii) In the enzyme environment the Fe−S bond is generally slightly longer than in the gas phase. (iv) In the quartet and sextet states the sulfur atom carries significantly more unpaired spin density in the gas phase than in the enzyme environment. This indicates that the enzyme environment favors localization of electron density on sulfur.

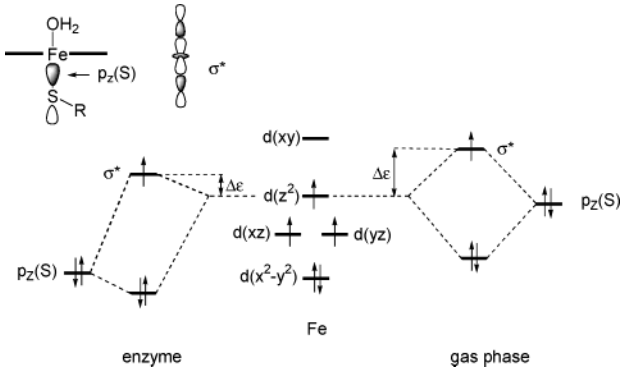

Figure 7. MO mixing diagram concerning the stabilization of the quartet (^{4}A) state by the polarizing effect of the enzyme (shown on the left) as compared to the gas phase (shown on the right).

The largest influence of the protein/solvent environment on energies, geometries, and spin densities is found for the quartet state. Particularly notable is the stabilization of the quartet (relative to the doublet) by electronic polarization (through the QM contributions); this effect is largest in the R1/B1 calculations. Figure 7 shows a MO diagram that rationalizes these findings in a simple manner.

Decisive for the relative stability of the quartet vs the doublet configuration is (in first approximation) the relative energy of the d(z^2) orbital with respect to the d(*xz*) orbital. If this energy difference is large, spin pairing (doublet state) will be preferred over occupation of the higher d(z^2) orbital (quartet state), which gives rise to a larger exchange stabilization. However, the d(z^2) orbital mixes with the p(*z*) orbital on sulfur and also with a corresponding orbital on the oxygen of the axial water ligand, yielding a bonding σ and an antibonding σ^* orbital (see Figure 7). The polarizing effect of the enzyme and the presence of H-bond donors in the Cys357 loop stabilize electronic charge on the sulfur atom, as has already been shown for the compound I species.[21] In the present case, this effectively lowers the orbital energy of the (doubly occupied) sulfur p(*z*) orbital. As a consequence, the interaction of this orbital with the d(z^2) orbital becomes weaker (see Figure 7), and therefore, the splitting of the bonding σ and antibonding σ^* orbital is smaller, as compared to the gas phase. Hence, the destabilization $\Delta\epsilon$ of the σ^* orbital (relative to the unperturbed d(z^2) orbital) due to the mixing is smaller and its occupation (and thus the quartet state) becomes more favorable, which is mirrored by the smaller calculated doublet−quartet gap in the enzyme environment. This accounts for a stabilization of the quartet state (by up to 10 kcal/mol in the case of R1/B1). When the calculations employ cysteinate (QM region R2) instead of SH^-, the effect is less pronounced, which mirrors the fact that cysteinate is a weaker σ-donor, i.e., the p(*z*) orbital on sulfur has a weaker interaction with d(z^2) even in the gas phase, thus leading to a smaller destabilization of σ^*. The donor properties of the sulfur ligand and its consequences for several aspects of P450 catalysis have been previously analyzed in detail on the basis of DFT calculations.[39]

The stabilization of the quartet state discussed here accords well with DFT single-point calculations by Scherlis et al.,[15] who

found a decrease of the vertical doublet−quartet gap by 7 kcal/mol when the polarizing effect of the protein was included into the QM treatment (DFT, BP86 functional) via an electrostatic interaction model similar to the one used here. To underscore this qualitative explanation we give the following properties computed (R1/B1) in the enzyme and in the gas phase. (i) The relative energy of the occupied α-spin Kohn−Sham orbitals in the quartet state corresponding to d(z^2) (σ*) and d(xz) orbitals: This gap is increased from 0.848 eV in the enzyme to 1.057 eV in the gas phase, which indicates that the polarizing environment predominantly lowers the orbital energy of the σ* orbital. (ii) The total Mulliken population on the sulfur: The electron population is decreased from 16.45 e in the enzyme environment to 16.20 e in the gas phase. This demonstrates that the enzyme environment effects localization of electron density on the sulfur atom (mainly through hydrogen bonding; see ref 21 for further discussion). Because the σ* orbital is unoccupied in the doublet state, the corresponding populations in this state are smaller (16.24 and 16.02). Hence, the quartet state will preferentially benefit from this effect. On the basis of these findings, one may also rationalize the differences in the Fe−S and Fe−O bond lengths between the enzyme and the gas phase. The argument is similar to the concept of the well-known trans-effect: two different donor ligands to a transition metal in trans orientation "compete" in forming a bond with the same orbital of the metal, in this case the d(z^2) orbital. Generally, the better σ-donor forms the stronger bond, while the bond to the other ligand is more labile as compared to the situation with identical ligands ("trans-effect"). In the present situation, the thiolate sulfur is clearly the stronger donor. However, the interaction of the sulfur p(z) orbital with the d(z^2) orbital is weakened by the enzyme environment, because the energetic separation between the two orbitals becomes larger (see Figure 7). As a consequence, the interaction of the d(z^2) orbital with the "competing" water ligand becomes stronger in the enzyme environment. In effect, the Fe−S bond is elongated, and the Fe−O bond is shortened in the protein as compared to the gas phase.

5. Conclusion

We report a comprehensive theoretical investigation of the energetic, geometric, and electronic factors that typify the resting form of $P450_{cam}$. In the first part, we have probed the dependence of the computed relative spin state energies on the chosen density functional. We find that the doublet, quartet, and sextet state energies are very sensitive to the admixture of exact exchange. Consistent with recent systematic work,[16,17] we conclude that pure density functionals such as BP86 or BLYP overestimate the stability of the LS state. B3LYP/CHARMM calculations for the full system indicate a doublet ground state, in accord with experimental results. Since the B3LYP functional is known to slightly underestimate the stability of the LS,[9,16,17,37] the calculated doublet−quartet and doublet−sextet gaps of ca. 2 and 3 kcal/mol may be regarded as a lower bound to the true values. Comparing the QM/MM results to analogous results for the isolated QM subsystem in the gas phase reveals the effects of the protein environment on the central iron−aqua complex, which may be summarized as follows: (i) The presence of other water molecules in the active site provides a hydrogen-bonding network that favors the upright conformation (perpendicular to the heme plane) of the axial water ligand. (ii) Electronic polarization of the QM part due to the enzyme environment stabilizes electron density on the proximal sulfur, which effectively lowers the orbital energy of the antibonding Fe−S σ* orbital. This provides a differential stabilization of the quartet state in the enzyme. (iii) The electronic polarization by the protein reduces the σ-donor capabilities of the sulfur ligand. This weakens and lengthens the Fe−S bond which, due to the trans-effect, causes a concomitant shortening of the Fe−O bond to the axial water ligand.

Our QM/MM calculations reveal how the protein/solvent environment modulates the conformation and binding properties of the axial water as well as the relative energies of the different spin states. This highlights the advantage of the combined QM/MM approach to simultaneously model the electronic factors at the heme site and the steric and electrostatic influence of the environment.

Acknowledgment. This research was supported by the Binational German Israeli Foundation (GIF). We thank Frank Neese for helpful discussions. J.C.S. thanks the Fonds der Chemischen Industrie for a Kekulé scholarship.

Supporting Information Available: Details of the setup procedure, force field parameters, and preparatory force field calculations. This material is available free of charge via the Internet at http://pubs.acs.org

References and Notes

(1) Ortiz de Montellano, P. R., Ed.; *Cytochrome P450: Structure, Mechanisms and Biochemistry*, 2nd ed.; Plenum Press: New York, 1995; Vol. 2.
(2) Dawson, J. H.; Sono, M. *Chem. Rev.* **1987**, *87*, 1255.
(3) Poulos, T. L.; Finzel, B. C.; Howard, A. J. *Biochemistry* **1986**, *25*, 5314.
(4) Thomann, H.; Berndardo, M.; Goldfarb, D.; Kroneck, P. M. H.; Ullrich, V. *J. Am. Chem. Soc.* **1995**, *117*, 8243.
(5) Goldfarb, D.; Bernardo, M.; Thomann, H.; Kroneck, P. M. H.; Ullrich, V. *J. Am. Chem. Soc.* **1996**, *118*, 2686.
(6) Tsai, R.; Yu, C. A.; Gunsalus, I. C.; Peisach, J.; Blumberg, W.; Orme-Johnson, W. H.; Beinert, H. *Proc. Natl. Acad. Sci. U.S.A.* **1970**, *66*, 1157.
(7) Sharrock, M.; Debrunner, P. G.; Schulz, C.; Lipscomb, J. D.; Marshall, V.; Gunsalus, I. C.*Biochim. Biophys. Acta* **1976**, *420*, 8.
(8) (a) Sligar, S. G.; Gunsalus, I. C. *Proc. Natl. Acad. Sci. U.S.A.* **1976**, *73*, 1078. (b) Sligar, S. G. *Biochemistry* **1976**, *15*, 5399. (c) Sligar, S. G.; Gunsalus, I. C. *Biochemistry* **1979**, *18*, 2290.
(9) Loew, G. H.; Harris, D. L. *Chem. Rev.* **2000**, *100*, 407.
(10) (a) Scheidt, W. R.; Cohen, I. A.; Kastner, M. E. *Biochemistry* **1979**, *18*, 3564. (b) Aissaoui, H.; Bachmann, R.; Schweiger, A.; Woggon, W.-D. *Angew. Chem., Int. Ed. Engl.* **1998**, *37*, 2998. (c) Woggon, W.-D. *Top. Curr. Chem.* **1996**, *184*, 39. (d) Woggon, W.-D.; Wagenknecht, H.-A.; Claude, C. *J. Inorg. Biochem.* **2001**, *83*, 289.
(11) Harris, D.; Loew, G. *J. Am. Chem. Soc.* **1993**, *115*, 8775.
(12) Segall, M. D.; Payne, M. C.; Ellis, S. W.; Tucker, G. T.; Boyes, R. N. *Phys. Rev. E* **1998**, *57*, 4618.
(13) Green, M. T. *J. Am. Chem. Soc.* **1998**, *120*, 10722.
(14) Filatov, M.; Harris, N.; Shaik, S. *J. Chem. Soc., Perkin Trans.* **1999**, *2*, 399.
(15) Scherlis, D. A.; Marti, M.; Ordejon, P.; Estrin, D. A. *Int. J. Quantum Chem.* **2002**, *90*, 1505.
(16) Reiher, M.; Salomon, O.; Hess, B. A. *Theor. Chem. Acc.* **2001**, *107*, 48.
(17) Salomon, O.; Reiher, M.; Hess, B. A. *J. Chem. Phys.* **2002**, *117*, 4729.
(18) Schlichting, I.; Berendzen, J.; Chu, K.; Stock, A. M.; Maves, S. A.; Benson, D. A.; Sweet, R. M.; Ringe, D.; Petsko, G. A.; Sligar, S. G. *Science* **2000**, *287*, 1615.
(19) Brooks, B. R.; Burccoleri, R. E.; Olafson, B. D.; States D. J.; Karplus, M. *J. Comput. Chem.* **1983**, *4*, 187.
(20) CHARMM22 force field: MacKerell, A. D., Jr.; Bashford, D.; Bellott, M.; Dunbrack, R. L., Jr.; Evanseck, J. D.; Field, M. J.; Fischer, S.; Gao, J.; Guo, H.; Ha, S.; Joseph-McCarthy, D.; Kuchnir, L.; Kuczera, K.; Lau, F. T. K.; Mattos, C.; Michnick, S.; Ngo, T.; Nguyen, D. T.; Prodhom, B.; Reiher, W. E., III; Roux, B.; Schlenkrich, M.; Smith, J. C.; Stote, R.; Straub, J.; Watanabe, M.; Wiorkiewicz-Kuczera, J.; Yin, D.; Karplus, M. *J. Phys. Chem. B* **1998**, *102*, 3586.
(21) Schöneboom, J. C.; Lin, H.; Reuter, N.; Thiel, W.; Cohen, S.; Ogliaro, F.; Shaik, S. *J. Am. Chem. Soc.* **2002**, *124*, 8142.
(22) Lounnas, V.; Wade, R. C. *Biochemistry* **1997**, *36*, 5402.
(23) Sherwood, P.; de Vries, A. H.; Guest, M. F.; Schreckenbach, G.; Catlow, C. R. A.; French, S. A.; Sokol, A. A.; Bromley, S. T.; Thiel, W.;

Turner, A. J.; Billeter, S.; Terstegen, F.; Thiel, S.; Kendrick, J.; Rogers, S. C.; Casci, J.; Watson, M.; King, F.; Karlsen, E.; Sjovoll, M.; Fahmi, A.; Schäfer, A.; Lennartz, C. *J. Mol. Struct. (THEOCHEM)* **2003**, *632*, 1.

(24) Becke, A. D. *Phys. Rev. A* **1988**, *38*, 3098.

(25) Becke, A. D. *J. Chem. Phys.* **1993**, *98*, 5648.

(26) Becke, A. D. *J. Chem. Phys.* **1993**, *98*, 1372.

(27) Lee, C.; Yang, W.; Parr, R. G. *Phys. Rev. B* **1988**, *37*, 785.

(28) Hay, J. P.; Wadt, W. R. *J. Chem. Phys.* **1985**, *82*, 299.

(29) (a) Ditchfield, R.; Hehre, W. J.; Pople, J. A. *J. Chem. Phys.* **1971**, *54*, 724. (b) Hehre, W. J.; Ditchfield, R.; Pople, J. A. *J. Chem. Phys.* **1972**, *56*, 2257. (c) Hariharan, P. C.; Pople, J. A. *Theor. Chim. Acta* **1973**, *28*, 213. (d) Clark, T.; Chandrasekhar, J.; Spitznagel, G. W.; Schleyer, P. v. R. *J. Comput. Chem.* **1983**, *4*, 294.

(30) Bakowies, D.; Thiel, W. *J. Phys. Chem.* **1996**, *100*, 10580.

(31) Antes, I.; Thiel, W. *Hybrid Quantum Mechanical and Molecular Mechanical Methods*; Gao, J., Ed.; ACS Symposium Series 712; American Chemical Society: Washington, DC, 1998; pp 50−65.

(32) de Vries, A. H.; Sherwood, P.; Collins, S. J.; Rigby, A. M.; Rigutto, M.; Kramer, G. J. *J. Phys. Chem. B* **1999**, *103*, 6133.

(33) (a) Ahlrichs, R.; Bär, M.; Häser, M.; Horn, H.; Kölmel, C. *Chem. Phys. Lett.* **1989**, *162*, 165. (b) Ahlrichs, R.; Bär, M.; Baron, H.-P.; Bauernschmitt, R.; Böcker, S.; Ehrig, M.; Eichkorn, K.; Elliot, S.; Furche, F.; Häser, M.; Horn, H.; Hättig, C.; Huber, C.; Huniar, U.; Kattanneck, M.; Köhn, A.; Kölmel, C.; Kollwitz, M.; May, K.; Ochsenfeld, C.; Öhm, H.; Schäfer, A.; Schneider, U.; Treutler, O.; v. Arnim, M.; Weigend, F.; Weis, P.; Weiss, H. *TURBOMOLE 5.5*; University of Karlsruhe, 2002.

(34) ChemShell is a modular QM/MM program developed in the European QUASI project under the coordination of P. Sherwood (see http://www.cse.clrc.ac.uk/qcg/chemshell).

(35) Smith, W.; Forester, T. *J. Mol. Graph.* **1996**, *14*, 136.

(36) Billeter, S. R.; Turner, A. J.; Thiel, W. *Phys. Chem. Chem. Phys.* **2000**, *2*, 2177.

(37) Scherlis, D. A.; Estrin, D. A. *Int. J. Quantum Chem.* **2002**, *87*, 158.

(38) Schöneboom, J. C.; Neese, F.; Thiel, W. Manuscript in preparation.

(39) (a) Ogliaro, F.; Cohen, S.; Filatov, M.; Harris, N.; Shaik, S. *Angew. Chem., Int. Ed.* **2000**, *39*, 3851. (b) Ogliaro, F.; Harris, N.; Cohen, S.; Filatov, M.; de Visser, S.; Shaik, S. *J. Am. Chem. Soc.* **2000**, *122*, 8977. (c) Ogliaro, F.; Cohen, S.; de Visser, S.; Shaik, S. *J. Am. Chem. Soc.* **2000**, *122*, 12892. (d) Ogliaro, F.; de Visser, S.; Shaik, S. *J. Inorg. Biochem.* **2003**, *91*, 554.